CONDENSED MATTER PHYSICS

Antiferromagnetic switching driven by the collective dynamics of a coexisting spin glass

Eran Maniv[1,2]*, Nityan L. Nair[1,2], Shannon C. Haley[1,2], Spencer Doyle[1,2], Caolan John[1,2], Stefano Cabrini[3], Ariel Maniv[4,5], Sanath K. Ramakrishna[5], Yun-Long Tang[1,2,6], Peter Ercius[3], Ramamoorthy Ramesh[1,2,6], Yaroslav Tserkovnyak[7], Arneil P. Reyes[5], James G. Analytis[1,2]*

The theory behind the electrical switching of antiferromagnets is premised on the existence of a well-defined broken symmetry state that can be rotated to encode information. A spin glass is, in many ways, the antithesis of this state, characterized by an ergodic landscape of nearly degenerate magnetic configurations, choosing to freeze into a distribution of these in a manner that is seemingly bereft of information. Here, we show that the coexistence of spin glass and antiferromagnetic order allows a novel mechanism to facilitate the switching of the antiferromagnet $Fe_{1/3 + \delta}NbS_2$, rooted in the electrically stimulated collective winding of the spin glass. The local texture of the spin glass opens an anisotropic channel of interaction that can be used to rotate the equilibrium orientation of the antiferromagnetic state. Manipulating antiferromagnetic spin textures using a spin glass' collective dynamics opens the field of antiferromagnetic spintronics to new material platforms with complex magnetic textures.

INTRODUCTION

There are a handful of material systems whose antiferromagnetic (AFM) spin texture can be electrically manipulated or "switched" (1–3). The mechanism is generally explained with the same underlying physics: An applied current induces a spin polarization due to a combination of inversion asymmetry and spin-orbit coupling that then transfers angular momentum into the system, exerting a "spin-orbit torque" that is able to manipulate the magnetic domains of the ordered state. Technically, this is referred to as a rotation of the Néel vector, which defines the orientation of a domain (4–6). This, in turn, rotates the principal axes of the conductivity of the material, providing a switch between high- and low-resistance states along perpendicular directions. The "high/low" contrast of the switching is determined not only by the efficacy with which angular momentum can be transferred to the magnetic lattice by the applied current but also by the degree of conductivity anisotropy within a domain.

The system $Fe_{1/3}NbS_2$ lacks inversion symmetry, so the spin-orbit coupling will cause a partial spin polarization of a current pulse (7, 8). In Fig. 1, we show the basic eight-terminal device configuration fabricated from single crystals of $Fe_{1/3 + \delta}NbS_2$ (see Materials and Methods for synthesis and focused ion beam microstructuring). In Fig. 1 (B and C), we illustrate "pulse trains" for two off-stoichiometry compositions, $x = 0.31$ and $x = 0.35$. Successive vertical and horizontal pulses take the system from high- to low-resistance states just as in other switchable AFMs but with two key differences (1, 2). First, there is single-pulse saturation of the signal, independent of the current density used, with no detectable relaxation to some intermediate resistance. Second, the pulse widths and current densities used are orders of magnitude lower than other systems, typically $\sim 10^6$ A/cm^2, whereas we observe switching at $\sim 10^4$ A/cm^2 (1, 2). Both these properties have obvious advantages technologically, but it is far from understood why these occur in this material but not in others. In this study, we show that the answer to this question is, unexpectedly, disorder. Disorder spawns a spin glass with its own collective dynamics (9), capable of transferring angular momentum to the coexisting AFM (10). There is one curious observation that distinguishes the compositions shown in Fig. 1: The electrical switching has a different phase for $x = 0.31$ than for $x = 0.35$. The Néel vector is being oriented in perpendicular directions in the dilute and excess iron compounds under the same direction of the current pulse. We shall revisit this observation later.

RESULTS

Although the Néel order is mostly oriented out of plane (11), the high- and low- resistance states are likely associated with the reorientation of a small in-plane component. This appears to be associated with an order parameter that causes a second transition at a lower temperature $T_{N'}$, appearing as a larger heat capacity anomaly (see Fig. 2B). In-plane studies of the nuclear magnetic resonance (NMR) confirm the presence of an in-plane component to the AFM order (see the Supplementary Materials). This is also confirmed by measurements of a zero-field anisotropic magnetoresistance (zAMR), shown in Fig. 1 (D to F), where cooling in an in-plane field permanently reorients the in-plane Néel vector. The zAMR consistently onsets at $T_{N'}$, consonant with the association of this transition with the in-plane canting of the moments. The zAMR, in principle, reflects the same conductivity as the high/low states of switching: a convolution of the average orientation of the in-plane Néel vector and the degree of anisotropy in the domain conductivity (12, 13).

In Figs. 2 and 3, we compare the temperature-dependent properties of the $x = 0.31$ and $x = 0.35$ compositions to stoichiometric samples near $x = \frac{1}{3}$. The thermodynamic properties are straightforward;

[1]Department of Physics, University of California, Berkeley, CA 94720, USA. [2]Materials Science Division, Lawrence Berkeley National Laboratory, Berkeley, CA 94720, USA. [3]Molecular Foundry, Lawrence Berkeley National Laboratory, Berkeley, CA 94720, USA. [4]NRCN, P.O. Box 9001, Beer Sheva, 84190, Israel. [5]National High Magnetic Field Laboratory, Tallahassee, FL 32310, USA. [6]Department of Materials Science and Engineering, University of California, Berkeley, CA 94720, USA. [7]Department of Physics and Astronomy, University of California, Los Angeles, Los Angeles, CA 90095, USA.
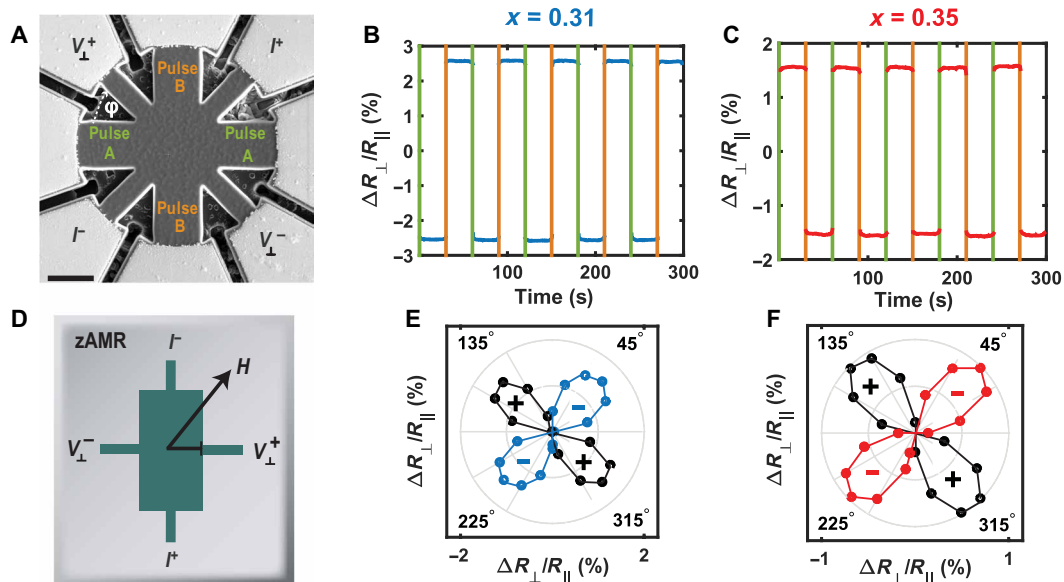*Corresponding author. Email: eranmaniv@berkeley.edu (E.M.); analytis@berkeley.edu (J.G.A.)

Fig. 1. The electrical switching and zero-field anisotropic magnetoresistance effects. (**A**) Scanning electron microscope image of a standard focused ion beam device fabricated. The ac contact configuration and the dc pulses are marked on top of the image. Scale bar, 10 μm. (**B** and **C**) Electrical current switching response measured at 2 K for $x = 0.31$ and $x = 0.35$ intercalations, respectively. A sequence of five A-B pulses was applied with a 30-s delay between pulses. The dc pulse amplitude was set at 54 kA/cm^2 (63 kA/cm^2) for the $x = 0.31$ ($x = 0.35$) intercalation for a duration of 10 ms. The A and B pulses are plotted as green and orange lines, respectively. An opposite response to the pulse sequence between both intercalations is observed. (**D**) Illustration of a typical ac contact configuration measured to probe the zero-field anisotropic magnetoresistance (zAMR) effect. (**E** and **F**) Angle-dependent polar plots of the zAMR effect measured at 2 K for $x = 0.31$ and $x = 0.35$ intercalations, respectively. The samples were cooled in a magnetic field of 9 T, at various in-plane angles (ϕ). Subsequently reaching base temperature, the magnetic field was turned off, and the transverse resistance ($R_\perp$) was measured. Black circles represent a positive zAMR response, while blue (red) circles represent a negative response for $x = 0.31$ ($x = 0.35$). A similar zAMR response between the two compositions is observed.
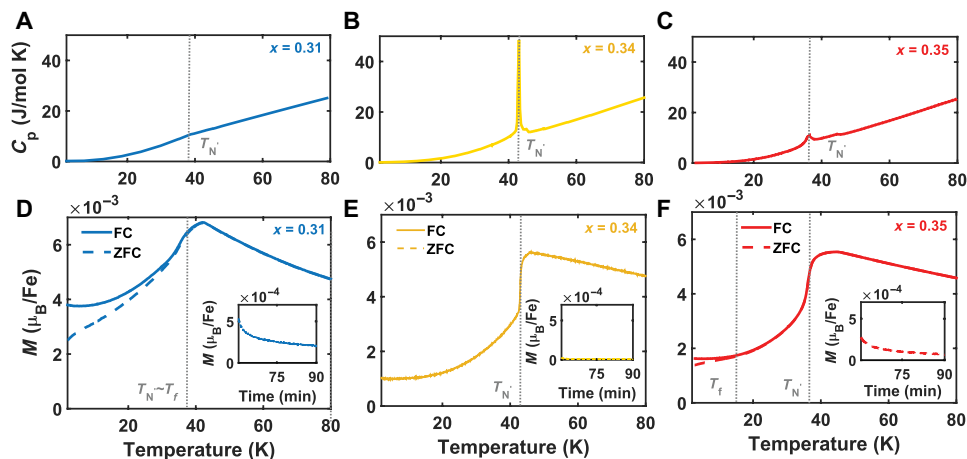

Fig. 2. Thermodynamic characterization of Fe$_x$NbS$_2$ for $x = 0.31$, $x = 0.34$, and $x = 0.35$. (**A** to **C**) Heat capacity versus temperature curves for all intercalation values measured without an applied magnetic field. The dotted line marks the lower AFM transition ($T_{N'}$), associated with an in-plane order. The vanishing heat capacity anomalies away from $x = 1/3$ are correlated with the entrance of a glassy state. (**D** to **F**) Magnetization (1000 Oe) versus temperature curves for each intercalation value: Both the field cool (FC: solid lines) and zero-field cool (ZFC: dashed lines) curves are presented. The magnetic field was applied in the perpendicular direction with respect to the NbS$_2$ layers (c axis). The divergence of the FC and ZFC curves demonstrates the onset of glassy behavior, i.e., the spin glass freezing temperature (T_f). Insets: Relaxation of the magnetization for $x = 0.31$, $x = 0.34$, and $x = 0.35$ intercalations at 5 K after a 1-T field was applied for 1 hour. The measurement is presented after the magnetic field was removed. Further analysis related to glassy dynamics is presented in the Supplementary Materials.

the $x = 0.34$ system has the largest and sharpest heat capacity and magnetic anomaly at the Néel transition $T_{N'}$, broadening substantially at compositions off-stoichiometry (14, 15). The magnetic susceptibility also shows that spin glass dynamics are only present off-stoichiometry, manifested as slow relaxation of the magnetiza-

tion (see insets of Fig. 2, D to F). The sensitivity of the spin glass to its history causes the field-cooled and zero field–cooled curves to separate at a characteristic freezing temperature T_f, an effect absent in $x = 0.34$, as observed in Fig. 2 (D and F) (16). Other effects characteristic of glassy dynamics including aging and hysteresis about
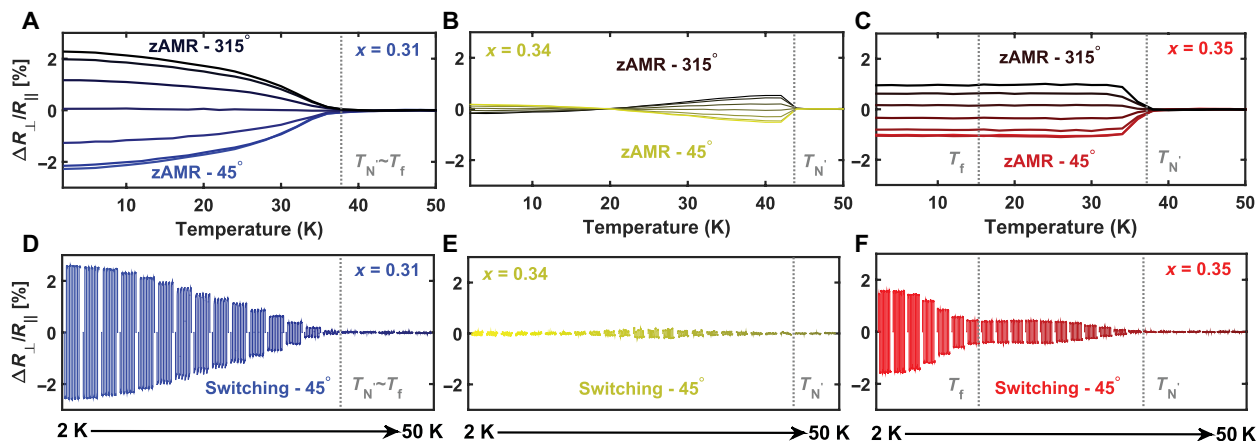
Fig. 3. Electrical switching and zAMR temperature dependencies. The temperature-dependent zAMR measurements of $x = 0.31$ (**A**), $x = 0.34$ (**B**), and $x = 0.35$ (**C**) intercalations are plotted. The FC angle window (zAMR 315° to 45° measured in steps of 15°), for each intercalation, is presented along the correlated curves. The zAMR onset corresponds to the AFM transition temperature ($T_{N'}$), with no distinct response to the spin glass freezing temperature (T_f). In the lower panels, we plot the electrical current switching response of $x = 0.31$ (**D**), $x = 0.34$ (**E**), and $x = 0.35$ (**F**) intercalations as a function of temperature. All switching devices were probed in the "switching 45°" configuration with a 100-μA (0.1 to 0.3 kA/cm^2) ac. All three plots are scaled similarly for comparison. To achieve switching, current densities of the order of 40 to 80 kA/cm^2 and pulse widths of the order of 1 to 10 ms were applied. For more information regarding pulse amplitude and width dependence, see the Supplementary Materials. For $x = 0.35$ (F), an enhanced switching response appears at the same temperature where the spin glass state starts to freeze (T_f). We note that the presented zAMR curves are not fully saturated (A to C), compared to the fully saturated switching response (D to F).

zero field are also present at these compositions (see the Supplementary Materials) (*17*). The temperature dependence of the zAMR signal (Fig. 3, A to C) passes through the freezing of the spin glass with impunity, reflecting only the smooth growth of the AFM order parameter as the temperature is lowered. Because the spin glass is invisible to the zAMR, it provides a reference point for the AFM response, untethered to the spin glass.

The temperature dependence of the electrical switching of the Néel vector offers an unexpected contrast to the thermodynamic response: It is strongly suppressed for compounds near stoichiometry and, in all respects, enhanced when the spin glass is present (Fig. 3, D to F). The interplay of spin glass and AFM order is especially pronounced in the $x = 0.35$ composition. Notice that although the Néel canting transition occurs at $T_{N'} \sim 37$ K, there is a large enhancement of the switching at $\sim$15 K (Fig. 3F). There is no (re) ordering phase transition in this range, but it is exactly the temperature where the spin glass freezes, T_f. At $x = 0.31$, T_f and $T_{N'}$ coincide, so that the switching simply follows the growth of the AFM order parameter (Fig. 3D). The data in Fig. 3 also illustrate another important point: The switching of stoichiometric compositions is not only substantially smaller than in the diluted or excess case but also substantially less stable. As can be observed in the enlargement at low temperatures (Fig. 4, A, E, and I), the signal for the $x = 0.34$ intercalation varies from pulse to pulse by up to 20%, in comparison to intercalations where the spin glass is present, where the signal is stable within 0.5%. The coexistence of the spin glass greatly increases the efficacy of the spin current in transferring angular momentum to the system, leading to an enhancement in both amplitude and stability of the switching. The switching of $Fe_{1/3 + \delta}NbS_2$ therefore depends on the interplay of the responses of two coupled order parameters, the AFM and the spin glass.

To better understand the mechanism of this interplay, we study the local environment of magnetic moments with NMR, shown in Fig. 4 (C, G, and K). The iron exchange field is studied via its effect on the ^{93}Nb lattice (with nuclear spin $I = 9/2$, $\gamma = 10.405$ MHz/T). In

the paramagnetic state at temperatures $T > T_{N'}$, the spectra exhibit a broad peak with quadrupolar splitting originating from two Nb unit cell sites. Below $T_{N'}$, the system splits into a double-peak structure symmetric about the paramagnetic center. This is a signature of AFM order, with the two peaks originating from the two sublattices where the hyperfine field ($\sim$1 T) adds to, and subtracts from, the applied magnetic field (*18*). Although the peak structure is broadly the same at all compositions (reflecting a similar AFM order for all x), on cooling in an out-of-plane field, an important difference emerges for compositions that are off-stoichiometry; the peaks become asymmetric in magnitude. The uncompensated moment of the spin glass influences the AFM sublattices below the freezing temperature, causing this asymmetry between the two peaks. For the nonglassy intercalation ($x = 0.33$), field cooling and zero-field cooling resulted in a symmetric two-peak structure, as expected for a pure AFM. This strongly suggests that the spin glass exerts an exchange field on the AFM lattice, causing spin flips that align with one sublattice. Moreover, since it is always the left-most peak that is enhanced, the exchange coupling J of the spin glass to its AFM neighbors is likely ferromagnetic (FM; $J > 0$) for both dilute and excess compositions. This provides strong evidence for the exchange coupling between the spin glass and the AFM order parameters.

DISCUSSION
The above data establish three facts about the nature of the switching in $Fe_{1/3 + \delta}NbS_2$ that distinguishes this system from any known counterpart. First, for a spin-polarized current to rotate the Néel state of the system with any efficacy, the system needs to be disordered; the spin glass must be present. This distinguishes the Néel rotation due to switching from that caused by applied field in the zAMR, which is not affected by the spin glass. Second, there is a local exchange interaction that couples the spin glass to the AFM lattice. Third, the freezing of the spin glass has the dual effect of enhancing
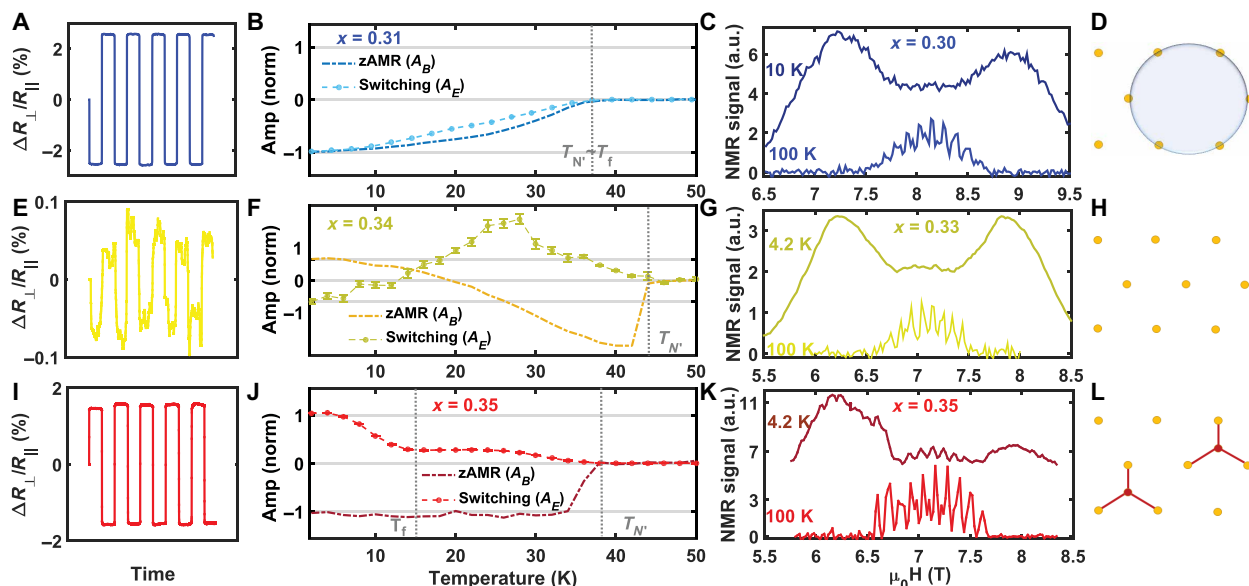
Fig. 4. Summary and NMR measurements. The low-temperature switching for $x = 0.31$ (**A**), 0.34 (**E**), and 0.35 (**I**) illustrates the stability and enhanced response while departing $x = 1/3$ value. Comparison between the electrical switching (full circles) and zAMR (dashed-dotted lines) temperature dependence for $x = 0.31$ (**B**), $x = 0.34$ (**F**), and $x = 0.35$ (**J**) is presented. Both switching (A_E) and zAMR (A_B) amplitudes are normalized by their low-temperature absolute value for comparison. The sign of the switching amplitude, low-high [sgn(A_E)= − 1] or high-low [sgn(A_E)= + 1] can be seen to depend on intercalation x and, for the sample near $x = 1/3$, on temperature, too. The transition from a correlated switching zAMR temperature dependence (B; $x = 0.31$) to an anticorrelated temperature dependence (J; $x = 0.35$) is clearly elucidated. See Materials and Methods for full definitions of the switching/zAMR responses and amplitudes. Field-swept ^{93}Nb NMR spectra at 85 MHz (**C**; $x = 0.30$) and 74.5 MHz (**G** and **K**; $x = 0.33$ and 0.35) were measured above and below the AFM transition. a.u., arbitrary units. All sweeps were performed after cooling the samples in a perpendicular magnetic field (c axis). In the paramagnetic regime, the field sweeps show the ^{93}Nb quadrupolar splitting for all intercalations. At low temperatures, two broad peaks indicative of a long-range AFM order emerge. For $x = 0.30$ (C) and $x = 0.35$ (K) samples, an asymmetry component appears on top of the low-temperature peaks. An illustration of the iron lattice is presented for the relevant regimes: vacancies (**D**), stoichiometric (**H**), and interstitials (**L**).

the current-induced rotation of the Néel state and then pinning it to create a large and stable high/low contrast.

To understand what is special about the coexistence of the spin glass and the AFM, it is notable that, in most examples of switchable AFMs, the switching does not saturate with a single pulse but rather shows saw-tooth behavior (1, 2). This is explained by assuming that most of the response is driven by shifts in the AFM domain boundaries (19, 20), the motion of which will change the average direction of the Néel vector. Domain boundaries generally form near structural defects in the material, and so, the switching depends on the ability of these defects to depin and move through the AFM lattice. Moreover, increased disorder will tend to make the electron scattering more isotropic, which will usually reduce the high/low contrast of the switching (7). The present situation appears, at first sight, to be in the opposite limit; not only do defects need to be present, but also the associated spin glass needs to be frozen ($T < T_f$) for the switching to become pronounced and stable. This implies that the freezing of the spin glass opens a new channel for the transfer of angular momentum, one that leverages the local stiffness of the spin glass itself.

The connection to stiffness suggests that the collective motion of the spin glass is transferring the spin torque. A related concept to this has been discussed in the context of spin hydrodynamics of insulating correlated spin glasses (10). The essential idea can be understood by describing the spin glass as a rotation matrix–valued order parameter describing an overall orientation of a volume of mutually disordered but frozen spins [this follows the treatment introduced by Halperin and Saslow (9) where this object can be

connected to the Edwards-Anderson order parameter of a spin glass]. A spin accumulation will generate a collective winding of this volume of spins, which is completely analogous to spin torques across interfaces (21), with a precession frequency that depends on the ratio of the relevant spin-mixing conductance and the Gilbert damping of the spin glass. In principle, if there is a coexisting AFM, as in the present case, then collective motion imparts spin torque on the Néel vector. Although the magnetic disorder and associated local anisotropies mean that spin is not conserved locally, the spin texture is topologically constrained by its spatiotemporal winding characteristics, with the net spin being the generator of the winding (10). The winding dynamics thus appears as a net nonequilibrium spin, amplifying the spin transfer from the electronic spin accumulation of the current pulse.

This mechanism may also help explain another unusual feature in the switching of $Fe_{1/3 + \delta}NbS_2$, briefly introduced in Fig. 1: The sign of δ determines which direction the Néel vector is rotated during the current pulse. Dilute compositions (δ < 0), where the defects are predominantly vacancies, switch in the opposite direction to excess compositions (δ > 0), where defects are likely to be interstitials. These defects would only weakly affect the structure, and extensive transmission electron microscopy (TEM) studies appear consistent with this identification, showing high intralayer structural order even for dilute compositions (see the Supplementary Materials). From the data, the following empirical correlation can be discerned

$$\text{sgn}(A_E) = -\text{sgn}(A_B) \times \text{sgn}(\delta) \tag{1}$$

where A_E (A_B) is the difference in resistivity $\Delta R_\perp / R_{//}$ observed in a switching (zAMR) experiment between vertical and horizontal electric pulses (applied magnetic fields). All compositions studied are consistent with this equation at all temperatures (Supplementary Materials). As noted above, the parameter A_B is sensitive only to the AFM order parameter, indifferent to the presence of the spin glass, whose sign measures the orientation of the Néel vector. The parameter δ in Eq. 1 therefore plays the role of a $\mathcal{Z}_2$ nematic field, whose sign determines the equilibrium orientation of the Néel vector after an electrical pulse, as reflected by the sign of A_E. Three-state nematicity has been found to exist in this compound on nonfabricated samples, indicating that it should play a role in the switching mechanism (22). This suggests that the local dynamics of the spin glass causes the Néel vector to either be rotated toward or away from the applied current pulse. The mechanism behind this must originate from differences in the microscopic spin texture of the spin glass in dilute and excess compositions; for example, there may be differences in FM clustering that exchange-bias the response of the AFM (23) or perhaps the helicity of the spin texture about the defects changes (24), distorting in orthogonal directions in the presence of an electrically driven spin accumulation. Whatever the magnetic texture dynamics responsible, the conclusion that the spin is being imparted by the spin glass, with a direction determined by the microscopic nature of the spin glass, is inescapable.

The coupled response of the AFM and spin glass order parameters is unambiguous in the data and is a substantial departure from the usual mechanism driving spin-orbit torque-based electrical switching of AFMs. The mechanism shares some commonality with FM/AFM heterostructures that leverage the spin angular momentum of the FM order and, in some cases, its magnons (25–26). In the present case, the collective behavior arises from the correlations between the defect species with its spinful environment. It would be interesting to study whether this collective dynamics can additionally excite collective modes (the so-called Halperin-Saslow modes), but future experiments of nonlocal transport are necessary to confirm their existence (27). Nevertheless, the collective behavior below T_f opens up a new channel of spin transfer and maximizes the efficacy with which angular momentum is imparted to the AFM by the current pulse, making the spin glass an essential partner in the switching mechanism. It is worth noting as a concluding remark that while spin glasses have been of extensive theoretical interest in condensed matter physics, they have been near absent in their application. The present work shows that while this mechanism is an uncommon way to leverage a spin glass to electrically switch an AFM, it need not be unique to $Fe_{1/3 + \delta}NbS_2$; correlated spin glasses appear generically in frustrated magnets (28), opening the field to candidate platforms that are in equal measure of applied and fundamental interest.

MATERIALS AND METHODS

Single crystals of Fe_xNbS_2 were synthesized using a chemical vapor transport technique. A polycrystalline precursor was prepared from iron, niobium, and sulfur in the ratio x:1:2 (Fe:Nb:S). The resulting polycrystalline product was then placed in an evacuated quartz ampoule with iodine as a transport agent (2.2 mg/cm^3) and put in the hot end of a two-zone MTI furnace with temperature set points of 800˚ and 950˚C for a period of 7 days. High-quality hexagonal crystals with diameters of several millimeters were obtained. The iron

intercalation values were confirmed by inductively coupled plasma optical emission spectroscopy (ICP-OES) using a PerkinElmer Optima 7000 DV ICP-OES system and energy-dispersive x-ray spectroscopy using an Oxford Instruments X-MaxN 50-mm^2 system. To perform the ICP-OES, the samples were first digested in hot 65% nitric acid, which was subsequently treated with an excess of HF to ensure complete dissolution of niobium, and the solutions were subsequently diluted to appropriate concentrations. Powder x-ray diffraction measurements were performed using a Rigaku Ultima-4 system with a Cu K-α radiation. High-angle annular dark-field (HAADF)–scanning TEM (STEM) images were recorded using the TEAM I at the Molecular Foundry: an aberration-corrected STEM (Thermo Fisher Scientific Titan Cubed, 80 to 300 kV) fitted with a high-brightness field-emission gun (X-FEG), a CEOS DCOR probe corrector operated at 300 kV. The beam convergence angle was 30 mrad and thus yields a probe size of less than 0.10 nm under STEM mode. Low-field magnetization measurements were performed using a Quantum Design Magnetic Property Measurement System-3 system with a maximum applied magnetic field of 7 T. Heat capacity was measured in a Quantum Design DynaCool Physical Property Measurement System system. Electrical pulses were achieved using a Keithley 6221 current source. NMR measurements were performed using the spin-echo technique, in the Condensed Matter NMR laboratory at the National High Magnetic Field Laboratory, using a home-built NMR spectrometer with quadrature detection. The magnetic field was varied between 6 and 10 T at various temperatures from 4.2 to 100 K. For the thermodynamic, zAMR and NMR measurements bulk single crystals were used. The switching devices required fabrication of bulk crystals into defined microstructures using a focused ion beam microscope as described in our previous study (3). The devices were fabricated in the a-b plane of the Fe_xNbS_2 crystal. All switching devices presented in the main text (in the Results section) were measured by the switching 45˚ configuration (presented in Fig. 1A). The switching and zAMR responses ($\Delta R_\perp / R_{//}$) are calculated by subtracting an average background from the measured transverse resistance ($R_\perp - R_{Avg}$) and normalizing to the longitudinal resistance ($R_{//}$) measured simultaneously. The switching amplitude (A_E) is defined as the difference in the relative resistivity change $\Delta R_\perp / R_{//}$ between A and B pulses. The zAMR amplitude (A_B) is defined as the difference in the relative resistivity change $\Delta R_\perp / R_{//}$ between $\phi = 45˚$ and $\phi = 135˚$.

SUPPLEMENTARY MATERIALS

Supplementary material for this article is available at http://advances.sciencemag.org/cgi/content/full/7/2/eabd8452/DC1

REFERENCES AND NOTES

1. P. Wadley, B. Howells, J. Železný, C. Andrews, V. Hills, R. P. Campion, V. Novák, K. Olejník, F. Maccherozzi, S. S. Dhesi, S. Y. Martin, T. Wagner, J. Wunderlich, F. Freimuth, Y. Mokrousov, J. Kuneš, J. S. Chauhan, M. J. Grzybowski, A. W. Rushforth, K. W. Edmonds, B. L. Gallagher, T. Jungwirth, Electrical switching of an antiferromagnet. *Science* **351**, 587–590 (2016).
2. S. Y. Bodnar, L. Šmejkal, I. Turek, T. Jungwirth, O. Gomonay, J. Sinova, A. A. Sapozhnik, H.-J. Elmers, M. Kläui, M. Jourdan, Writing and reading antiferromagnetic Mn$_2$Au by Néel spin-orbit torques and large anisotropic magnetoresistance. *Nat. Commun.* **9**, 348 (2018).
3. N. L. Nair, E. Maniv, C. John, S. Doyle, J. Orenstein, J. G. Analytis, Electrical switching in a magnetically intercalated transition metal dichalcogenide. *Nat. Mater.* **19**, 153–157 (2020).
4. H. V. Gomonay, V. M. Loktev, Spin transfer and current-induced switching in antiferromagnets. *Phys. Rev. B* **81**, 144427 (2010).
5. J. Železný, H. Gao, K. Výborný, J. Zemen, J. Mašek, A. Manchon, J. Wunderlich, J. Sinova, T. Jungwirth, Relativistic néel-order fields induced by electrical current in antiferromagnets. *Phys. Rev. Lett.* **113**, 157201 (2014).

6. O. Gomonay, T. Jungwirth, J. Sinova, Concepts of antiferromagnetic spintronics. *Phys. Status Solidi* **11**, 1700022–1702017

7. V. Baltz, A. Manchon, M. Tsoi, T. Moriyama, T. Ono, Y. Tserkovnyak, Antiferromagnetic spintronics. *Rev. Mod. Phys.* **90**, 015005 (2018).

8. V. M. Edelstein, Spin polarization of conduction electrons induced by electric current in two-dimensional asymmetric electron systems. *Solid State Commun.* **73**, 233–235 (1990).

9. B. Halperin, W. Saslow, Hydrodynamic theory of spin waves in spin glasses and other systems with noncollinear spin orientations. *Phys. Rev. B* **16**, 2154–2162 (1977).

10. H. Ochoa, R. Zarzuela, Y. Tserkovnyak, Spin hydrodynamics in amorphous magnets. *Phys. Rev. B* **98**, 054424 (2018).

11. B. Van Laar, H. M. Rietveld, D. J. W. Ijdo, Magnetic and crystallographic structures of Me_xNbS_2 and Me_xTaS_2. *J. Solid State Chem.* **3**, 154–160 (1971).

12. D. Kriegner, K. Výborný, K. Olejník, H. Reichlová, V. Novák, X. Marti, J. Gazquez, V. Saidl, P. Němec, V. V. Volobuev, G. Springholz, V. Holý, T. Jungwirth, Multiple-stable anisotropic magnetoresistance memory in antiferromagnetic mnte. *Nat. Commun.* **7**, 11623 (2016).

13. J. Železný, P. Wadley, K. Olejník, A. Hoffmann, H. Ohno, Spin transport and spin torque in antiferromagnetic devices. *Nat. Phys.* **14**, 220–228 (2018).

14. T. Tsuji, Y. Yamamura, H. Watanabe, K. Saito, M. Sorai, Heat capacity of intercalated layered materials Fe_xNbS_2 at low temperature. *J. Therm. Anal. Calorim.* **57**, 839–846 (1999).

15. Y. Yamamura, S. Moriyama, T. Tsuji, Y. Iwasa, M. Koyano, S. Katayama, M. Ito, Heat capacity and phase transition of Fe_xNbS_2 at low temperature. *J. Alloys Compd.* **383**, 338–341 (2004).

16. N. Doi, Y. Tazuke, Spin Glass Phases in 2H-Fe_xNbS2. *J. Phys. Soc. Jpn.* **60**, 3980–3981 (1991).

17. J. A. Mydosh, *Spin Glasses: An Experimental Introduction* (CRC Press, 2014).

18. N. Büttgen, P. Kuhns, A. Prokofiev, A. P. Reyes, L. E. Svistov, High-field NMR of the quasi-one-dimensional antiferromagnet $LiCuVO_4$. *Phys. Rev. B* **85**, 214421 (2012).

19. Q. Li, G. Chen, T. P. Ma, J. Zhu, A. T. N'Diaye, L. Sun, T. Gu, Y. Huo, J. H. Liang, R. W. Li, C. Won, H. F. Ding, Z. Q. Qiu, Y. Z. Wu, Activation of antiferromagnetic domain switching in exchange-coupled Fe/CoO/MgO (001) systems. *Phys. Rev. B* **91**, 134428 (2015).

20. P. Wadley, S. Reimers, M. J. Grzybowski, C. Andrews, M. Wang, J. S. Chauhan, B. L. Gallagher, R. P. Campion, K. W. Edmonds, S. S. Dhesi, F. Maccherozzi, V. Novak, J. Wunderlich, T. Jungwirth, Current polarity-dependent manipulation of antiferromagnetic domains. *Nat. Nanotechnol.* **13**, 362–365 (2018).

21. Y. Tserkovnyak, H. Ochoa, Generalized boundary conditions for spin transfer. *Phys. Rev. B* **96**, 100402 (2017).

22. A. Little, C. Lee, C. John, S. Doyle, E. Maniv, N. L. Nair, W. Chen, D. Rees, J. W. F. Venderbos, R. M. Fernandes, J. G. Analytis, J. Orenstein, Three-state nematicity in the triangular lattice antiferromagnet $Fe_{1/3}NbS_2$. *Nat. Mater.* **19**, 1062–1067 (2020).

23. Y.-C. Lau, D. Betto, K. Rode, J. M. D. Coey, P. Stamenov, Spin–orbit torque switching without an external field using interlayer exchange coupling. *Nat. Nanotechnol.* **11**, 758–762 (2016).

24. O. Gomonay, V. Baltz, A. Brataas, Y. Tserkovnyak, Antiferromagnetic spin textures and dynamics. *Nat. Phys.* **14**, 213–216 (2018).

25. W. H. Meiklejohn, C. P. Bean, New magnetic anisotropy. *Phys. Rev.* **102**, 1413–1414 (1956).

26. J. Nogués, I. K. Schuller, Exchange bias. *J. Magn. Magn. Mater.* **192**, 203–232 (1999).

27. L. J. Cornelissen, J. Liu, R. A. Duine, J. B. Youssef, B. J. van Wees, Long-distance transport of magnon spin information in a magnetic insulator at room temperature. *Nat. Phys.* **11**, 1022–1026 (2015).

28. K. H. Fischer, J. A. Hertz, *Spin Glasses* (Cambridge Univ. Press, 1993), vol. 1.

29. E. Vincent, Ageing, rejuvenation and memory: The example of spin-glasses, in *Ageing and the Glass Transition*, M. Henkel, M. Pleimling, R. Sanctuary, Eds. (Springer, 2007), pp. 7–60.

30. Y. L. Tang, Y. L. Zhu, X. L. Ma, A. Y. Borisevich, A. N. Morozovska, E. A. Eliseev, W. Y. Wang, Y. J. Wang, Y. B. Xu, Z. D. Zhang, S. J. Pennycook, Observation of a periodic array of flux-closure quadrants in strained ferroelectric $PbTiO_3$ films. *Science* **348**, 547–551 (2015).

31. S. Das, Y. L. Tang, Z. Hong, M. A. P. Gonçalves, M. R. McCarter, C. Klewe, K. X. Nguyen, F. Gómez-Ortiz, P. Shafer, E. Arenholz, V. A. Stoica, S.-L. Hsu, B. Wang, C. Ophus, J. F. Liu, C. T. Nelson, S. Saremi, B. Prasad, A. B. Mei, D. G. Schlom, J. Íñiguez, P. García-Fernández, D. A. Muller, L. Q. Chen, J. Junquera, L. W. Martin, R. Ramesh, Observation of room-temperature polar skyrmions. *Nature* **568**, 368–372 (2019).

32. Y. L. Tang, Y. L. Zhu, Y. Liu, Y. J. Wang, X. L. Ma, Giant linear strain gradient with extremely low elastic energy in a perovskite nanostructure array. *Nat. Commun.* **8**, 15994 (2017).

Citation: E. Maniv, N. L. Nair, S. C. Haley, S. Doyle, C. John, S. Cabrini, A. Maniv, S. K. Ramakrishna, Y.-L. Tang, P. Ercius, R. Ramesh, Y. Tserkovnyak, A. P. Reyes, J. G. Analytis, Antiferromagnetic switching driven by the collective dynamics of a coexisting spin glass. *Sci. Adv.* **7**, eabd8452 (2021).